

Upgrading of pine tannin biochars as electrochemical capacitor electrodes

Sara Pérez-Rodríguez^{a,*}, Oscar Pinto^{b,c}, María T. Izquierdo^d, Cristina Segura^e, Po S. Poon^e, Alain Celzard^a, Juan Matos^{f,*}, Vanessa Fierro^{a,*}

^aUniversité de Lorraine, CNRS, IJL, F-88000, Epinal, France

^bDepartamento de Ingeniería Química, Facultad de Ingeniería, Universidad de Concepción, Barrio Universitario s/n, Chile.

^cANID–Millennium Science Initiative Program, Millennium Nuclei on Catalytic Process towards Sustainable Chemistry (CSC), Chile.

^dInstituto de Carboquímica (ICB-CSIC), Miguel Luesma Castan 4, E-50018 Zaragoza, Spain.

^eUnidad de Desarrollo Tecnológico (UDT), Universidad de Concepción, Barrio Universitario s/n, Concepción, Chile.

^fInstituto de Ciencias Químicas Aplicadas, Facultad de Ingeniería, Universidad Autónoma de Chile, 8900000 Santiago, Chile.

*Corresponding Authors:

S. Pérez-Rodríguez. Email: sara.perez-rodriguez@univ-lorraine.fr. Phone: +33 (0)372 749 677

J. Matos. Email: juan.matos@uautonoma.cl. Phone: +56 9 9379 8340

V. Fierro. Email: Vanessa.Fierro@univ-lorraine.fr. Phone: +33 (0)372 749 677

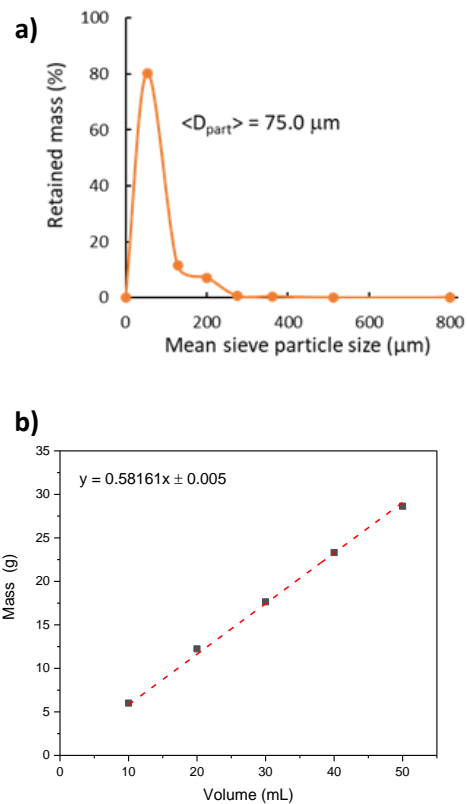


Figure S1. Characterization of tannin-derived biochars (TBC): (a) particle size distribution; and (b) determination of bulk density.

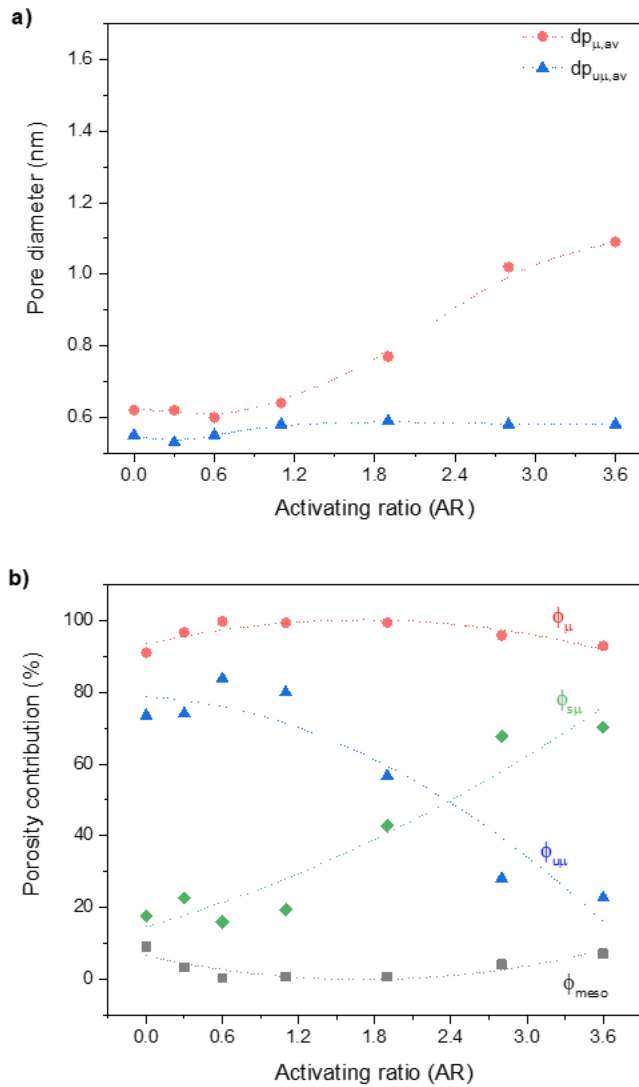


Figure S2. (a) Average micropore and ultramicropore sizes; and (b) mesopore (ϕ_{meso}), micropore (ϕ_μ), supermicropore ($\phi_{s\mu}$), and ultramicropore ($\phi_{u\mu}$) percentages as a function of activating ratio (AR), obtained from the NLDFT method combining both N_2 and CO_2 adsorption data of biochar-derived ACs.

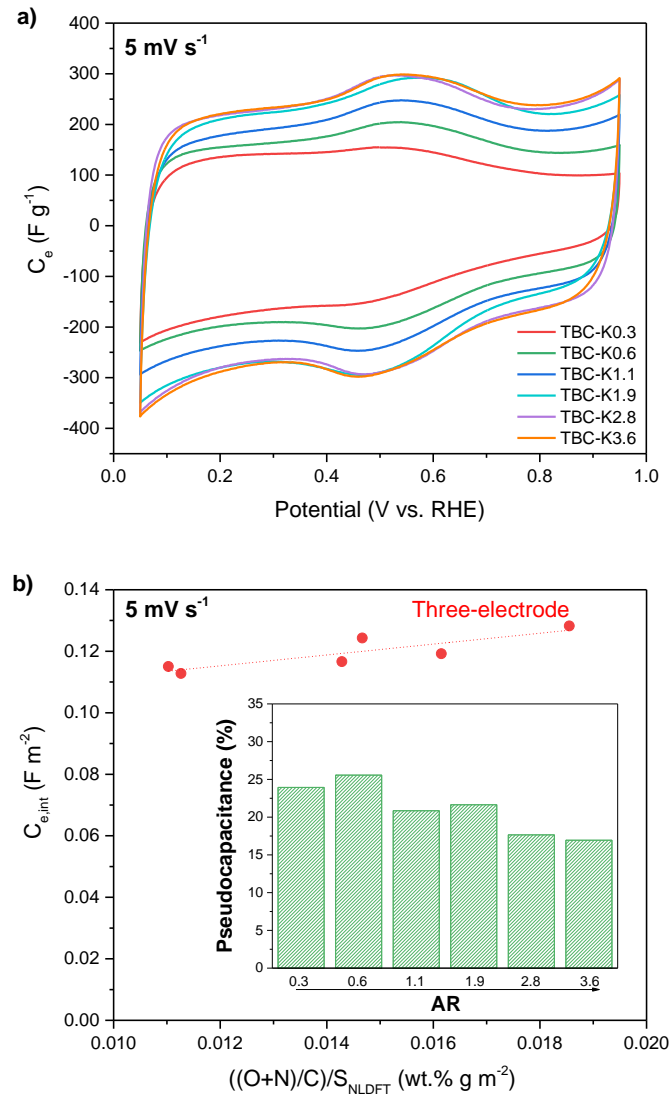


Figure S3. CV tests in a three-electrode electrochemical cell in aqueous electrolyte (1 M H_2SO_4) of biochar-derived ACs: (a) comparison of capacitance-potential curves at 5 mV s^{-1} ; (b) electrode capacitance normalized by S_{NLDFT} ($C_{e,int-3e}$) as a function of the $(\text{O+N})/\text{C}$ per S_{NLDFT} at 5 mV s^{-1} . The inset shows the pseudocapacitance contribution (%) at the different activating ratios (AR).

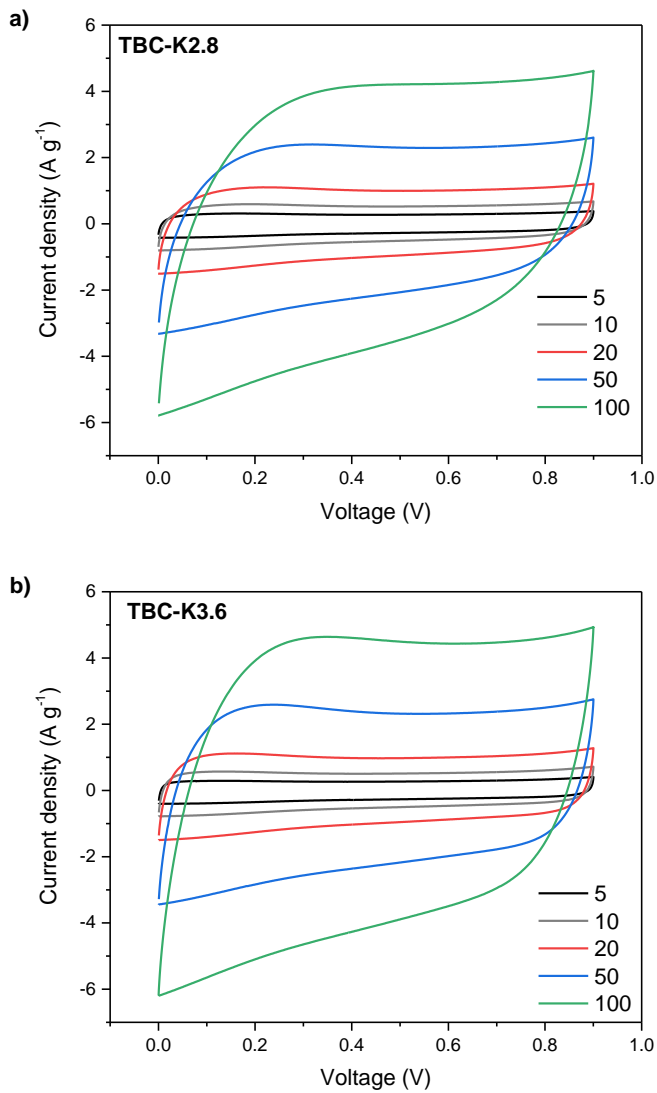


Figure S4. Cyclic voltammograms at different scan rates (mV s^{-1}) of symmetrical ECs in aqueous electrolyte (1 M H_2SO_4) based on: (a) TBC-K2.8; and (b) TBC-K3.6.

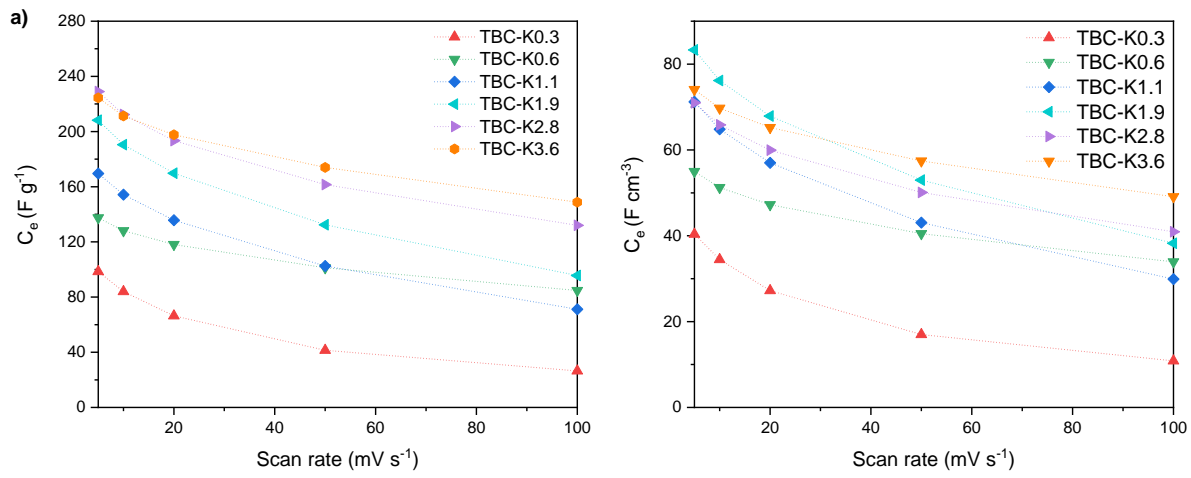


Figure S5. (a) Specific; and (b) volumetric electrode capacitance as a function of scan rate for symmetrical ECs based on biochar-derived ACs in aqueous electrolyte (1 M H_2SO_4).

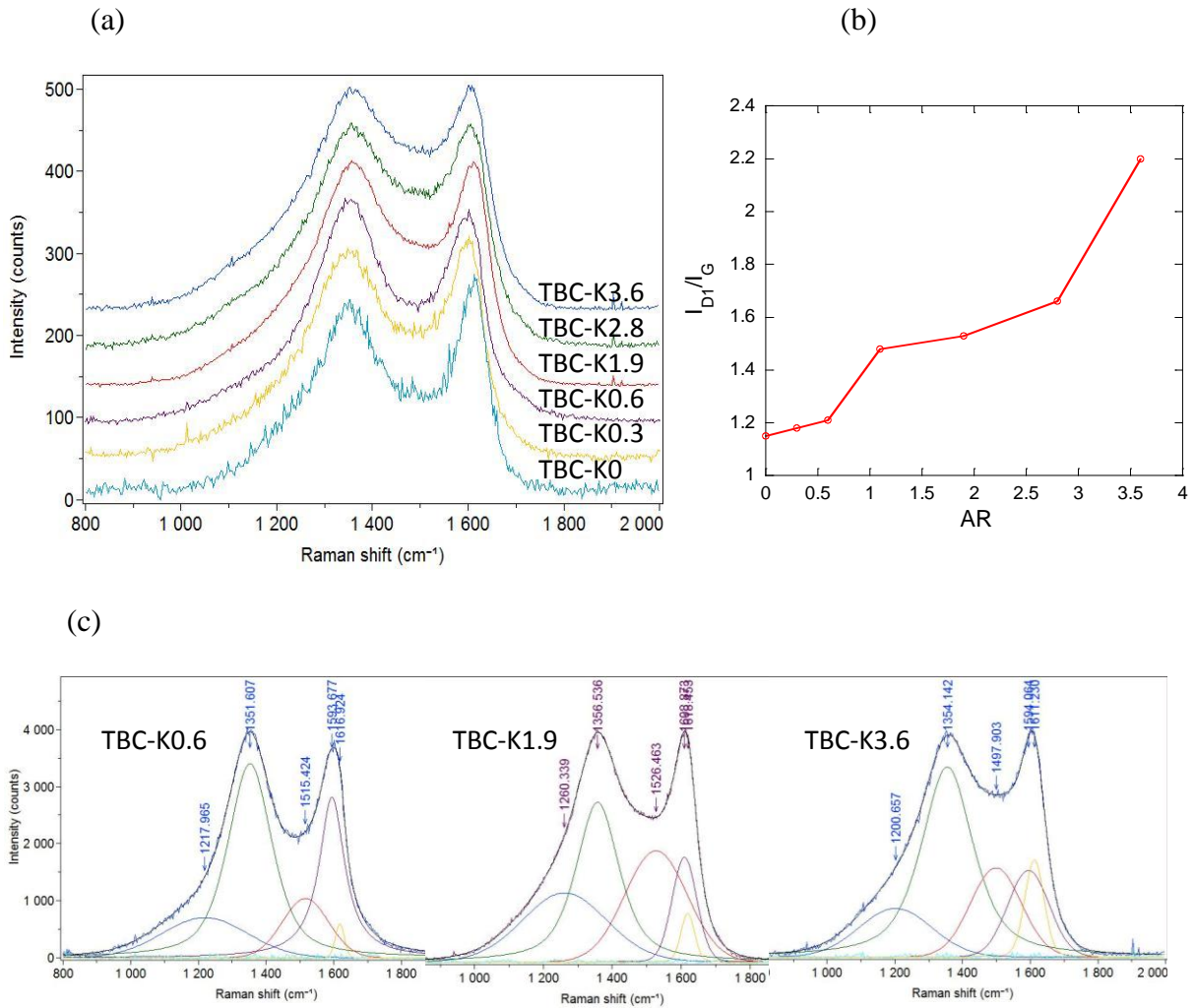


Figure S6. Raman spectra of biochar-derived ACs produced at different activating ratios: (a) raw profiles of, from bottom to top: TBC-K0, TBC-K0.3, TBC-K0.6, TBC-K1.9, TBC-K2.8 and TBC-K3.6; (b) Intensity ratios of bands D1 ($\sim 1350 \text{ cm}^{-1}$) to G ($\sim 1595 \text{ cm}^{-1}$); (c) Examples of deconvolution of Raman profiles into 5 bands, from left to right: TBC-K0.6, TBC-K1.9 and TBC-K3.6.

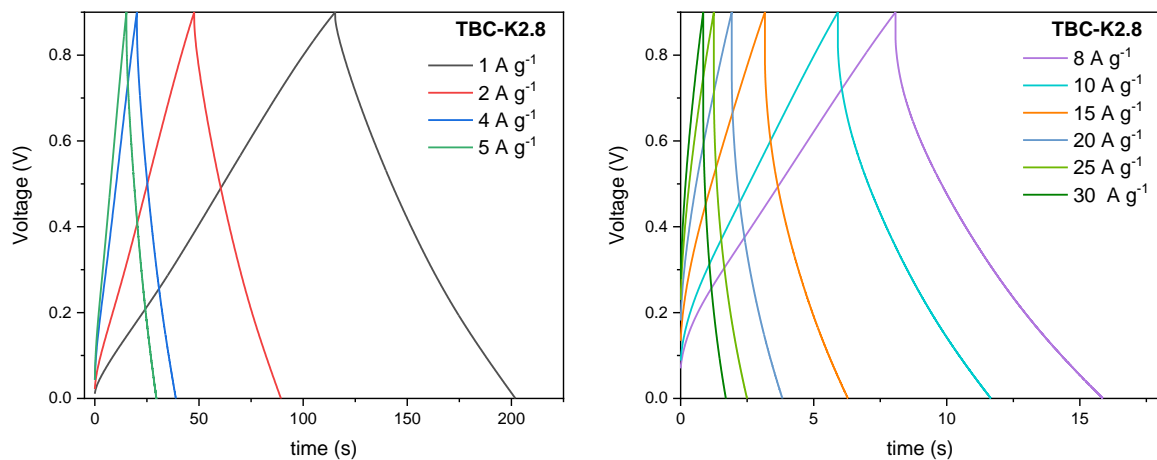


Figure S7. Galvanostatic charge-discharge profiles at several current densities for symmetrical TBC-K2.8-based EC in aqueous electrolyte (1 M H₂SO₄).

Table S1. Textural parameters calculated from N₂ and CO₂ adsorption isotherms and product yields of the biochar-derived ACs.^a

Sample	AR	A _{BET} (m ² g ⁻¹)	S _{NLDFT} (m ² g ⁻¹)	V _{0.97} (cm ³ g ⁻¹)	V _{DR,N2} (cm ³ g ⁻¹)	V _{DR,CO2} (cm ³ g ⁻¹)	V _{NLDFT} (cm ³ g ⁻¹)	V _{μ,NLDFT} (cm ³ g ⁻¹)	V _{uμ,NLDFT} (cm ³ g ⁻¹)	V _{meso,NLDFT} (cm ³ g ⁻¹)	V _{meso} (cm ³ g ⁻¹)	w _{av} (nm)	w _{μ,av} (nm)	w _{uμ,av} (nm)	Yield (%) ^b
TBC	-	384	623	0.17	0.15	0.18	0.21	0.18	0.12	0.02	0.02	1.81	0.69	0.52	44
TBC-K0	0.0	489	789	0.21	0.18	0.22	0.25	0.22	0.18	0.02	0.03	1.61	0.62	0.55	33 (74)
TBC-K0.3	0.3	599	1057	0.24	0.23	0.26	0.31	0.30	0.23	0.01	0.01	1.19	0.62	0.53	27 (61)
TBC-K0.6	0.6	808	1310	0.31	0.30	0.32	0.37	0.37	0.31	0.00	0.01	0.66	0.60	0.55	30 (69)
TBC-K1.1	1.1	1183	1625	0.46	0.45	0.41	0.49	0.49	0.39	0.00	0.02	0.75	0.64	0.58	30 (69)
TBC-K1.9	1.9	1783	1998	0.71	0.67	0.47	0.69	0.69	0.39	0.00	0.04	0.91	0.77	0.59	30 (68)
TBC-K2.8	2.8	2417	2190	1.04	0.85	0.43	0.97	0.92	0.27	0.04	0.20	1.22	1.02	0.58	26 (58)
TBC-K3.6	3.6	2554	2147	1.10	0.85	0.40	1.01	0.94	0.23	0.07	0.25	1.26	1.09	0.58	21 (48)

^a A_{BET}: BET area from the N₂ adsorption isotherms. V_{0.97}: total pore volume at a relative pressure of 0.97. V_{DR,N₂} and V_{DR,CO₂}: micropore volumes by application of the DR equation to the data obtained from the N₂ and CO₂ isotherms, respectively. V_{meso}: mesopore volume determined as V_{0.97} - V_{DR,N₂}. S_{NLDFT}: specific surface area by the 2D-NLDFT-HS model from N₂ and CO₂ adsorption isotherms. V_{NLDFT}, V_{μ,NLDFT} and V_{uμ,NLDFT}: total pore volume, micropore volume and ultramicropore volume, respectively, by application of the 2D-NLDFT-HS model to N₂ and CO₂ adsorption isotherms. V_{meso,NLDFT}: mesopore volume (V_{meso,NLDFT} = V_{NLDFT} - V_{μ,NLDFT}). w_{av}, w_{μ,av} and w_{uμ,av}: average widths of pores, micropores, and ultramicropores, respectively, by application of the 2D-NLDFT-HS model to N₂ and CO₂ adsorption isotherms.

^b Total yield, biochar activation yield is given in brackets.

Table S2. Bulk and surface chemical composition from elemental analysis (EA) and XPS, respectively, of biochar-derived ACs.

Sample	EA (wt.%)					XPS (wt.%)			XPS (at.%)			O_{XPS}/O_{EA}
	C	N	H	S*	O	C	N*	O	C	O	C/O	
TBC	80.6	0.1	2.7	Nd	14.8	89.5	Nd	10.5	91.9	8.1	8.5	0.71
TBC-K0	89.7	0.1	1.6	Nd	7.7	90.5	Nd	3.7	97.2	2.8	26.0	0.48
TBC-K0.3	82.6	0.4	1	Nd	13.7	84.6	Nd	15.4	88.0	12.0	5.5	1.12
TBC-K0.6	78.6	0.3	1.3	Nd	18.8	85.6	Nd	15.6	88.8	12.2	5.5	0.83
TBC-K1.1	81.4	0.2	0.9	Nd	19.2	84.5	Nd	15.5	87.9	12.1	5.4	0.81
TBC-K1.9	82.0	0.1	0.9	Nd	23.3	88.0	Nd	12.0	90.7	9.3	7.3	0.52
TBC-K2.8	83.1	0.1	0.8	Nd	20.4	90.2	Nd	9.8	92.5	7.5	9.3	0.48
TBC-K3.6	81.1	0.1	0.8	Nd	19.1	89.0	Nd	11.0	91.5	8.5	8.1	0.58

*Nd (not detected).

Table S3. Relative areas (%) of the deconvoluted peaks of C1s and O1s for biochar-derived ACs. The corresponding binding energies (eV) are shown in brackets.

Sample	C1s ^a					C1s ^b			
	C I	C II	C III	C IV	CV	O I	O II	O III	O IV
TBC	73.3 (284.4)	21.1 (285.5)	4.7 (287.6)	0.9 (289.2)	-	39.9 (531.5)	60.1 (533.3)	-	-
TBC-K0	74.3 (284.5)	19.7 (285.5)	3.7 (287.6)	1.3 (289.2)	-	44.2 (531.6)	54.6 (533.1)	1.2 (534.5)	-
TBC-K0.3	63.8 (284.5)	25.3 (285.6)	8.6 (287.6)	2.3 (289.1)	-	48.5 (531.1)	43.4 (532.9)	6.7 (534.5)	1.4 (536.5)
TBC-K0.6	64.5 (284.5)	24.4 (285.5)	8.8 (287.6)	2.2 (288.7)	-	65.7 (531.1)	29.3 (533.0)	5.0 (534.5)	-
TBC-K1.1	64.7 (284.4)	24.6 (285.5)	8.9 (287.7)	1.8 (288.8)	-	65.6 (531.1)	28.8 (533.1)	5.6 (534.5)	-
TBC-K1.9	63.5 (284.4)	26.2 (285.5)	8.7 (287.6)	1.6 (289.2)	-	54.4 (531.1)	38.1 (533.0)	7.5 (534.5)	-
TBC-K2.8	62.1 (284.5)	25.3 (285.6)	8.5 (287.6)	2.7 (289.1)	1.5 (290.4)	43.6 (531.1)	50.0 (532.9)	6.4 (535.0)	-
TBC-K3.6	62.4 (284.4)	26.6 (285.5)	7.8 (287.6)	2.0 (289.1)	1.3 (290.1)	24.9 (531.1)	67.7 (532.7)	7.4 (534.5)	-

^a**C I:** hydrocarbons, aromatics, aliphatics; **C II:** C-C sp³ carbon and C-O single bonds associated to ethers, phenols and anhydrides; **C III:** C=O double bonds in carbonyls and quinones; **C IV:** C-O single bonds in carboxyls; **CV:** plasmon loss or shake-up π-π satellite.

^b**O I:** C=O double bonds in quinone-type groups, carbonyls and carboxylic acids; **O II:** -OH bonds in phenols, C–O–C ether groups and C=O bonds in ester and anhydride groups; **O III:** single C-O bonds in esters and anhydrides, COOH carboxylic groups; **O IV:** chemisorbed oxygen and/or water